# A Finite Element Analysis of Masticatory Stress Hypotheses

Janine Chalk,[1,2]* Brian G. Richmond,[2,3] Callum F. Ross,[4] David S. Strait,[5] Barth W. Wright,[6] Mark A. Spencer,[7] Qian Wang,[8] and Paul C. Dechow[9]

[1]*Hominid Paleobiology Doctoral Program, Department of Anthropology, The George Washington University, Washington, DC 20052*
[2]*Center for the Advanced Study of Hominid Paleobiology, Department of Anthropology, The George Washington University, Washington, DC 20052*
[3]*Human Origins Program, National Museum of Natural History, Smithsonian Institution, Washington, DC 20560*
[4]*Department of Organismal Biology & Anatomy, University of Chicago, Chicago, IL 60637*
[5]*Department of Anthropology, State University of New York at Albany, Albany, NY 12222*
[6]*Department of Anatomy, Kansas City University of Medicine and Biosciences, Kansas City, MO 64106*
[7]*Institute of Human Origins, School of Human Evolution and Social Change, Arizona State University, Tempe, AZ 85287*
[8]*Division of Basic Medical Sciences, Mercer University School of Medicine, Macon, GA 31207*
[9]*Department of Biomedical Sciences, Baylor College of Dentistry, Texas A&M Health Science Center, Dallas, TX 75246*

*KEY WORDS* skull; feeding; biomechanics; bone strain; anthropoids

*ABSTRACT* Understanding how the skull transmits and dissipates forces during feeding provides insights into the selective pressures that may have driven the evolution of primate skull morphology. Traditionally, researchers have interpreted masticatory biomechanics in terms of simple global loading regimes applied to simple shapes (i.e., bending in sagittal and frontal planes, dorsoventral shear, and torsion of beams and cylinders). This study uses finite element analysis to examine the extent to which these geometric models provide accurate strain predictions in the face and evaluate whether simple global loading regimes predict strains that approximate the craniofacial deformation pattern observed during mastication. Loading regimes, including those simulating peak loads during molar chewing and those approximating the global loading regimes, were applied to a previously validated finite element model (FEM) of a macaque (*Macaca fascicularis*) skull, and the resulting strain patterns were compared. When simple global loading regimes are applied to the FEM, the resulting strains do not match those predicted by simple geometric models, suggesting that these models fail to generate accurate predictions of facial strain. Of the four loading regimes tested, bending in the frontal plane most closely approximates strain patterns in the circumorbital region and lateral face, apparently due to masseter muscle forces acting on the zygomatic arches. However, these results indicate that no single simple global loading regime satisfactorily accounts for the strain pattern found in the validated FEM. Instead, we propose that FE models replace simple cranial models when interpreting bone strain data and formulating hypotheses about craniofacial biomechanics. Am J Phys Anthropol 145:1–10, 2011. 

Much research into the relationship between feeding biomechanics and craniofacial morphology has focused on which loading regimes play the most important role in shaping craniofacial adaptation and how stresses are dissipated through the cranium. Early research on primate craniofacial biomechanics commonly conceptualized the skull as a simple geometric structure or system of structures (e.g., beams and cylinders) in efforts to interpret the adaptive significance of facial morphology and predict stress and strain in the face (Görke, 1904; Richter, 1920; Endo, 1966; Endo, 1973; Roberts and Tattersall, 1974; Demes, 1982; Greaves, 1985; Rangel et al., 1985; Preuschoft et al., 1986). Endo (1966, 1973) used a complex rigid frame model, which treated the skull as a series of interconnected straight beams, or members, of uniform cross section to predict internal stress patterns in the face, and tested the model with *in vitro* strain gage experiments in human and gorilla skulls. In his analyses, the skull was loaded with simulated bilateral temporalis and masseter muscles forces, reaction forces at the temporomandibular joints (TMJ), and a bite force applied to each tooth excluding the third molars (Endo, 1966). When these loading conditions were applied, the gorilla

Additional Supporting Information may be found in the online version of this article.

Grant sponsor: NSF; Grant number: 0240865; Grant sponsor: NSF HOMINID; Grant numbers: BCS-0725141 (P.C.D.); BCS-0725122 (B.G.R.); BCS-0725147 (C.F.R.); BCS-0725219 (M.A.S.); BCS-0725126 (D.S.S.); BCS-0725183 (Q.W.); BCS-0725136 (B.W.W.).

*Correspondence to: Janine Chalk, Department of Anthropology, The George Washington University 2110 G St., NW, Washington, DC 20052. E-mail: jchalk@gwmail.gwu.edu

Received 23 February 2010; accepted 3 September 2010

DOI 10.1002/ajpa.21416
Published online 26 October 2010 in Wiley Online Library (wileyonlinelibrary.com).

and human skulls exhibit a comparable pattern of deformation (Endo, 1966; Endo, 1970). The medial and lateral maxillozygomatic member, the regions above and lateral to the nasal aperture, and the medial and lateral aspects of the browridge were identified as areas subject to high bending moments. During simulations of the peak loads of unilateral chewing on the postcanine teeth, the experimental results and theoretical model suggested increased bending moments and compressive forces on the working side, whereas incisal bites increased bending moments and compression in regions near the midline of the face (Endo, 1966). From this and subsequent work four main hypotheses emerged regarding which loading regimes best characterize how forces act on the craniofacial skeleton (Fig. 1). These global loading regimes are 1) bending in the frontal plane (Endo, 1966; Endo, 1973; Russell, 1985; Picq and Hylander, 1989; Hylander et al., 1991b), 2) bending in the sagittal plane (Cartmill, 1974; Hylander, 1977; Demes, 1982; Preuschoft et al., 1986), 3) dorsoventral shear of the face relative to the braincase (Hylander, 1977; Demes, 1982; Preuschoft et al., 1986), and 4) torsion of the face on the braincase about the anteroposterior axis of the skull (Greaves, 1985; Greaves, 1995).

## GLOBAL LOADING REGIME PREDICTIONS

Bending of the primate face in the frontal plane results from superiorly directed bite forces applied to the anterior dentition and inferiorly directed bilateral temporalis and masseter muscle forces applied to the lateral aspects of the orbits and zygomatic arches (Fig. 1A) (Endo, 1966; Endo, 1970; Russell, 1985; Hylander et al., 1991a, b). When the supraorbital region is modeled as a simple beam, tensile strains are predicted to be perpendicular to the midsagittal plane of the skull, and magnitudes are predicted to be highest in the dorsal interorbital region (Fig. 1B) (Hylander et al., 1991b). The superiorly directed bite force is expected to yield compressive strain concentrations parallel to the midsagittal plane of the skull (Endo, 1966; Endo, 1970; Hylander et al., 1991a, b).

The predictions of bending in the sagittal plane are derived from modeling the skull as a triangular-shaped beam, perhaps better described as a truss. Hylander et al. (1991b) note that this loading regime is the result of superiorly directed bite forces at the teeth and joint reaction forces at the TMJs, combined with inferiorly directed masticatory muscle forces (Fig. 1C). The simple geometric model predicts tensile strains to occur along the palate extending to the pterygoid processes and the zygomatic arches. Compressive strains are expected to be concentrated in the dorsal face, including the maxilla and interorbital region (Fig. 1D) (Hylander et al., 1991b). Both tensile and compressive strains are predicted to be oriented parallel to the sagittal plane (Hylander et al., 1991b).

Similarly, dorsoventral shearing is caused by the superiorly directed bite and TMJ joint reaction forces and the inferiorly-directed masticatory muscle forces resulting in the displacement of the facial skeleton superiorly relative to the braincase (Fig. 1E). This superior displacement of the face in the sagittal plane is resisted by bone in the sagittal planes (i.e., between the face rostrally and the neurocranium caudally). Tensile strains are expected to occur in the dorsal and ventral aspects of the face, with rostral regions experiencing higher strains relative to areas with thicker bone such as the browridge (Fig. 1F). Dorsoventral shearing is also predicted to cause shear in the lateral surfaces of the rostrum and orbits (Preuschoft et al., 1986; Hylander et al., 1991b).

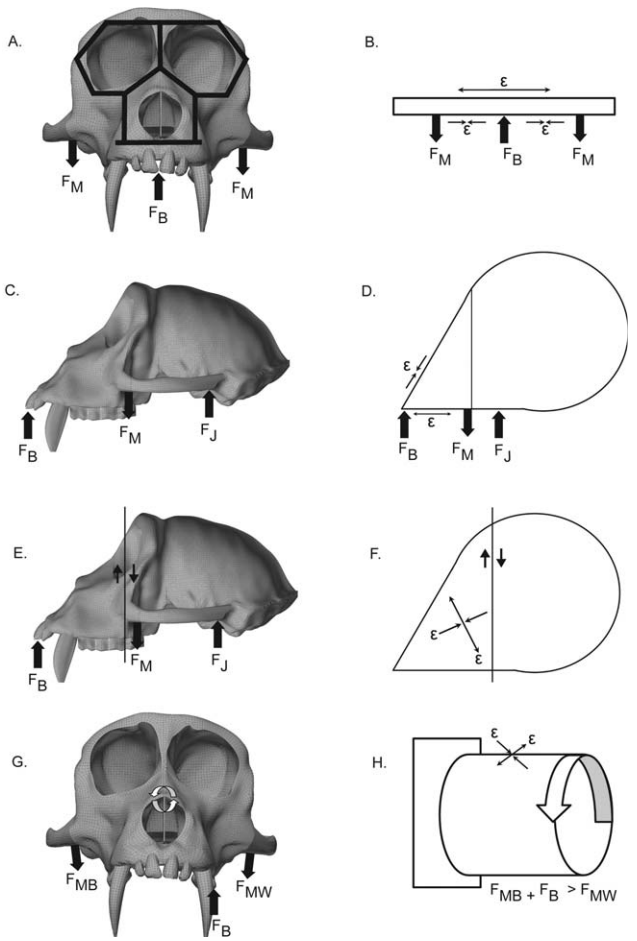


**Fig. 1.** The four proposed global loading regimes applied to the macaque skull and strain predictions from simple geometric models of the skull adapted from Hylander et al. (1991b). (**A**) Endo's (1966) rigid frame model superimposed on the macaque face. Bending in the frontal plane is the result of inferiorly directed muscle forces ($F_M$) and superiorly directed bite force ($F_B$); (**B**) Beam model of bending in the frontal plane, with arrows indicating the predicted strain pattern on the superior and inferior surface of the beam; (**C**) Bending in the sagittal plane is the result of inferiorly directed muscle forces ($F_M$) and joint reaction force ($F_J$) and superiorly directed bite force ($F_B$); (**D**) Model of a triangular-shaped beam bending in the sagittal plane, with arrows indicating the predicted strain pattern on the superior and inferior surfaces; (**E**) Dorsoventral shear is the result of inferiorly directed muscle forces ($F_M$) and superiorly directed joint reaction forces ($F_J$) and bite force ($F_B$). The arrows indicate the shear direction; (**F**) The skull model shearing in the frontal plane with arrows indicating the strain pattern on lateral surface; (**G**) Torsion of the face about the braincase is the result of bite force ($F_B$) and balancing side muscle force ($F_{MB}$) exceeding the working side muscle force ($F_{MW}$) causing a counter-clockwise twist; and (**H**) A cylinder undergoing a counter-clockwise twist. Arrows indicate the predicted strain pattern oriented 45° to the long axis of the cylinder.

Twisting of the face on the braincase about the anteroposterior axis of the skull is the final loading regime proposed to characterize the pattern of facial strain during mastication. Here, the face is modeled as a cylinder that twists during unilateral mastication as a result of the torsional moments of the balancing side muscle force and bite force exceeding the working side muscle force (Fig. 1G) (Greaves, 1985, 1995). In this loading regime, tensile and compressive strain orientations are predicted to be 45° to the twisting axis (i.e., the long-axis of the skull) (Fig. 1H) (Greaves, 1985; Hylander et al., 1991b; Greaves, 1995; Ross, 2001; Ross, 2008).

Although facial strain predictions derived from simple geometric models are compatible with *in vivo* bone strain data for the zygomatic arch and postorbital septum (Ross and Hylander, 1996; Hylander and Johnson, 1997), these simple models appear to provide accurate strain predictions only when the structure approximates the dimensions of the simple geometric model, withstands few external forces, and shows relatively homogeneous material properties (Ross, 2001). However, many facial structures, and certainly the face as a whole, do not satisfy these conditions, leading some researchers to argue that simple geometric models are an unreliable method of assessing stress and strain for these regions (Hylander et al., 1991b; Ross, 2001). In their *in vivo* bone strain analysis, Hylander et al. (1991b) tested the influence of these loading regimes in the supraorbital region of macaques and baboons and found some correspondence between *in vivo* strain directions at gage sites during incision and mastication and strains predicted from Endo's rigid frame model during bending in the frontal plane. Despite this support, Hylander et al. (1991b) contend that the morphological complexity of primate craniofacial structures precludes an accurate prediction of strain from simple geometric models of the skull. If their predictions are reliable, both frontal plane and sagittal plane bending models are consistent with strain patterns inferred from experimental data in the macaque supraorbital region (Hylander et al., 1991b), whereas parasagittal bending, transverse bending, and torsion models are consistent with the strain patterns observed in the zygomatic arch (Hylander and Johnson, 1997). Additional experimental data collected from the circumorbital region in owl monkeys, lemurs, and macaques indicate strain patterns in this region also do not conform to the predictions of a single loading regime (Ross and Hylander, 1996; Ross, 2001; Ross, 2008). Together these studies suggest that strain patterns in the face are consistent with multiple loading regimes.

In this study, we use finite element analysis (FEA) to investigate the extent to which simple assumptions regarding differing models of skull geometry and loading regimes yield accurate predictions about strain distributions in the primate craniofacial skeleton. Specifically, we use FEA to evaluate two hypotheses: 1) simple geometric models can provide accurate predictions of strain in the primate face and 2) a single global loading regime is primarily responsible for the pattern of craniofacial deformation in the macaque skull.

## MATERIALS AND METHODS

FEA provides a powerful approach to evaluating craniofacial deformation in response to masticatory stresses (Dumont et al., 2005; Metzger et al., 2005; Richmond et al., 2005; Strait et al., 2005; Rayfield, 2007; Kupczik et al., 2007; Strait et al., 2007; Kupczik et al., 2009; Strait et al., 2009; Strait et al., 2010; Wang et al., 2010a,b). Data collected from *in vivo* and *in vitro* bone strain experiments serve to validate the finite element model (FEM), ensuring the FEM reflects actual performance (Metzger et al., 2005; Strait et al., 2005; Rayfield, 2007; Wang et al., 2008). The model can thus be employed to evaluate the effects of mastication on the craniofacial morphology of primates and to refine biomechanical hypotheses (Richmond et al., 2005; Ross et al., 2005; Strait et al., 2005).

The FEM used in this study is a previously validated molar-loaded model of a male macaque (*Macaca fascicularis*) consisting of 311,057 polyhedral elements with orthotropic, regionally assigned material properties (Strait et al., 2005). In this validated FEM, the force magnitudes and orientations of eight masticatory muscles (right and left anterior temporalis, right and left masseter, and right and left medial pterygoid) were estimated from physiological cross-sectional data and relative muscle recruitment activity during normal mastication (Antón, 1993; Antón, 1999; Ross, 2001; Ross et al., 2005). To simulate the reaction forces at the TMJ, constraints were applied at the articular eminences. An additional constraint was placed at the left first molar, where a reaction force simulates the bite force.

In this study, four loading conditions (i.e., frontal bending, sagittal bending, dorsoventral shear, and torsion) were applied to the macaque FEM (Fig. 2A-D). Details concerning the external forces and constraints for each simple global loading regime are provided in Table 1 and shown in Figure 2. Constraints at the articular eminences preventing translation and rotation in all axes were applied to all of the FEMs, except dorsoventral shear where the braincase was constrained posterior to the browridge (Richmond et al., 2005; Strait et al., 2005) (Fig. 2C). The load applied to each loading regime FEM was the sum of the muscle force magnitudes applied to the validated FEM (200 Newtons). Because our aim is to test the biomechanical impact of each hypothesized global loading regime, loading regime models do not include biologically realistic muscle force directions or bite points. We applied external forces and constraints to the macaque FEM that were consistent with the force components of the four simple global loading regimes (frontal plane bending, sagittal plane bending, dorsoventral shear, and torsion) to produce models with deformations representing each global loading regime.

To model bending in the frontal plane, 200 N of force were applied in the -y direction (i.e., inferiorly) to the anterior region of the zygomatic arches. In addition to the TMJ, constraints to prevent translation and rotation were placed on the posterior palatal surface of the maxilla (Fig. 2A). To model bending in the sagittal plane, 200 N of force were applied in the −y direction at the occlusal surfaces of the third molars. The incisors were loaded with 200 N of force in the +y direction (Fig. 2B). In the FE modeling of dorsoventral shear, a frontal region of the skull was loaded with 200 N of force in the +y direction, while the neurocranium was constrained from translation and rotation (Fig. 2C). To model the torsion loading regime, the occlusal surface of the molars on the right side were loaded with 100 N in the

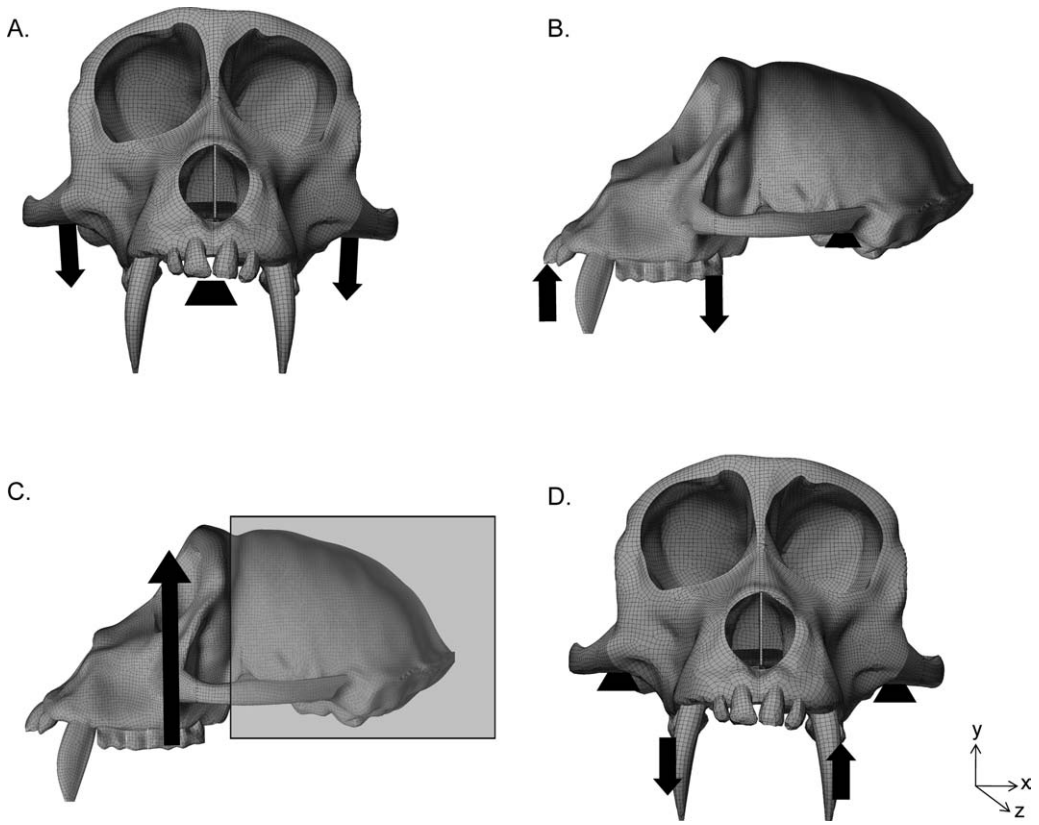


**Fig. 2.** Details of loads and constraints applied to the validated molar mastication FEM, simulating each of the proposed loading regimes. (**A**) To model bending in the frontal plane, 200 Newtons (N) of force were applied in the −y direction to the anterior region of the zygomatic arches. Superior and inferior forces were applied in the approximately the same coronal plane to ensure modeling pure bending in the frontal plane. Constraints were placed on the surface of the palate posterior to the incisive canal and at the articular eminences; (**B**) To model bending in the sagittal plane, 100 N of force were applied in the −y direction at the occlusal surfaces of the third molars. The incisors were loaded with 100 N of force in the +y direction. Constraints were placed at the articular eminences; (**C**) In the dorsoventral shear, the face was allowed to translate only in the y direction. A frontal section of the skull was loaded with 200 N of force in the +y direction. Constraints on the neurocranium prevent movement and induce pure shear; (**D**) The occlusal surface of the molars on the right side were loaded with 100 N in the −y direction, and the occlusal surface of the molars on the left side were loaded with 100 N of force in the +y direction. Constraints were applied at the articular eminences.

*TABLE 1. Description of boundary conditions applied to model the four simple global loading regimes*

| Global loading regime | Constraints | Forces |
|---|---|---|
| Frontal plane bending | Right and left TMJs (36 nodes; no translation or rotation; nodal $df = 0$); Posterior palate (272 nodes; no translation or rotation; nodal $df = 0$) | 200 N applied to right and left anterior zygomatic arches (1278 nodes; applied in −y direction) |
| Sagittal plane bending | Right and left TMJs (42 nodes; no translation or rotation; nodal $df = 0$) | 200 N applied to $M^3$ (213 nodes; applied in the +y direction); 200 N applied to central and lateral incisors (213 nodes; applied in the −y direction) |
| Dorsoventral shear | Braincase and posterior zygomatic arches (all surfaces constrained; no translation or rotation); facial region (2149 nodes; translation in y direction; nodal $df = 1$) | Facial region overlapping contrained nodes (561 nodes; applied in the +y direction) |
| Torsion | Right and left TMJs (42 nodes; no translation or rotation; nodal $df = 0$) | 200 N applied to right and left postcanine tooth row (1026 nodes; applied in the −y direction on the right and +y direction on the left) |

-y direction (Fig. 2D). The occlusal surface of the molars on the left side were loaded with 100 N of force in the +y direction. A counterclockwise twist was achieved by selecting an equal number of occlusal surface nodes on the left and right sides to ensure that an equal force was applied to each side of the model. This model was constrained from translation and rotation at the TMJs.

To compare the results of the four global loading regimes to those of the validated FEM, two sets of strain magnitude and orientation data were analyzed. The first data set involved collecting data from eight surface nodes in the dorsal orbital and infraorbital region, the zygomatic arches, and the working side postorbital bar. These eight regions were selected to correspond with the strain gage locations from which *in vivo* bone data have been collected from *M. fascicularis* and *M. mulatta* (Hylander et al., 1991b; Hylander and Johnson, 1997; Ross et al., 2002; Ross et al., in press). The purpose of comparing strain values estimated from these *in vivo* locations was to identify which of the global loading regimes most closely resembles the maximum principal strain orientation observed during normal chewing. The second data set involved constructing three additional nodal data sets to sample regions of the face beyond those areas with available experimental strain data. These node sets consist of a line of nodes along the lateral and superior aspect of the face, three anterior-posterior transects on the working and balancing side of the rostrum, and a line of nodes around the nasal aperture. In each of the analyses, principal components analysis (Statistica 7, StatSoft, Tulsa, OK) of strain orientation was used to compare the predictions of the global loading environments with the validated FEM. Principal components analysis was used to reduce the data retrieved from the five FEMs allowing us to identify which global loading regime most closely resembled the validated FEM.

## RESULTS

### Deformations Caused by the Global Loading Regimes

The results of the FEA of bending in the frontal plane show inferior displacement of the orbits, superior rostrum, and zygomatic arches (Fig. 3A). This FEM conforms in some respects to the strain pattern predicted by the simple geometric model (Fig. 1B and 3A). The lateral aspects of the face, especially the lateral orbital region and the zygomatic arches, experience tensile strains, whereas facial regions along the midsagittal plane, such as the interorbital region, experience compressive strains. However, tensile strain concentrations are also observed in the inferomedial orbital wall and the superior margin of the nasal cavity, which are not accurately represented when modeling the skull as a simple geometry such as a beam.

The results of the FEM of bending in the sagittal plane show a superior rotation of the face about the TMJ, with the most notable displacement in the anterior aspect of the snout (Fig. 3B). The simple model predicts tensile strains will be present in the palate and compressive strains will occur in the superior aspect of the rostrum (Fig. 1D). Concentrations of tensile strain occur along the maxilla and palate as well as on the dorsal aspect of the rostrum and the inferomedial and superolateral regions of the orbit. The FEM experiences compressive strains in the inferolateral orbital region and along the dorsal aspect of the rostrum, consistent with the predictions from the geometric model.

The overall pattern of deformation in the dorsoventral shear FEM demonstrates a superior displacement of the whole face relative to the braincase (Fig. 3C). The simple model of dorsoventral shear predicts the anterior regions of the face will experience increased shearing forces relative to the posterior regions of the face (i.e., the browridge) (Figs. 1E-F). Regions of the face adjacent to the plane of shear, such as the inferior orbital, superior orbital, and interorbital regions and the malar regions experience concentrations of tensile strain. Compared with those regions near the plane of shear, other areas of the face show relatively little tensile or compressive strains.

Results of the torsion FEM show a pattern of deformation in which the snout undergoes a counterclockwise twist about the anteroposterior axis of the skull (Figs. 1G-H and 3D). The right orbit and zygomatic arch are displaced inferiorly, whereas the left orbit and zygomatic arch experience a superiorly directed displacement. Concentrations of tensile strain are seen along the right side of the rostrum as well as the lateral and inferior aspects the right orbit and the superomedial aspect of the left orbit of the FEM. The most striking area of tension observed in the FEM occurs along the superior margin of the nasal cavity, which bends inward toward the midline. In contrast, compressive strains occur along inferior and lateral regions of the left orbit and the left zygomatic arch of the twisted FEM.

### Comparisons Between the Global and Masticatory Loading Regimes

Maximum principal strain ($\varepsilon_1$) orientation and maximum to minimum principal strain ratio ($\varepsilon_1/|\varepsilon_2|$) were considered to compare strain patterns from the FEMs of global loading regimes with the validated FEM at the eight nodes corresponding to locations with experimental data (Fig. 4A). In the principal components analysis of $\varepsilon_1$ orientation, the frontal bending and sagittal bending models lie closest to the validated FEM on the first two principal component axes, whereas the torsion and dorsoventral shear models produce strain patterns which differ substantially from that observed in the validated FEM (Fig. 4B). The first three principal components account for 96.5% of the total variance. Strain orientation in the infraorbital (Nodes 4 and 5), zygomatic arches (Nodes 6 and 7), and working side dorsal orbital (Node 2) regions drive the variation in the first three principal components. The frontal and sagittal bending FEMs group closely with the molar mastication FEM on principal components axes 1 and 2 (Fig. 4B). The factors driving the PC1 axis (52.4% of the variance) are in the working and balancing side infraorbital (Nodes 4 and 5) regions and the balancing side zygomatic (Node 7) (Supplementary table 1). The infraorbital nodes also contribute to the PC2 axis, which accounts for 33.2% of the variance. The global loading regime models do not cluster with the validated FEM on PC3 (10.2%), and nodes at the dorsal interorbital (Node 1), working side zygomatic (Node 6), and postorbital bar (Node 8) drive the variation on this axis (Fig. 4B). Comparison of the $\varepsilon_1/|\varepsilon_2|$ ratios reveal a similar pattern in which the strain produced in the frontal bending model best approximates the validated FEM (Fig. 5). The dispersion of $\varepsilon_1/|\varepsilon_2|$ ratios from experimental bone strain data compiled by Strait et al. (2005) are also shown in Figure 5. The variation from experimental data encompasses all models at the interorbital (Node 1) and dorsal working or-

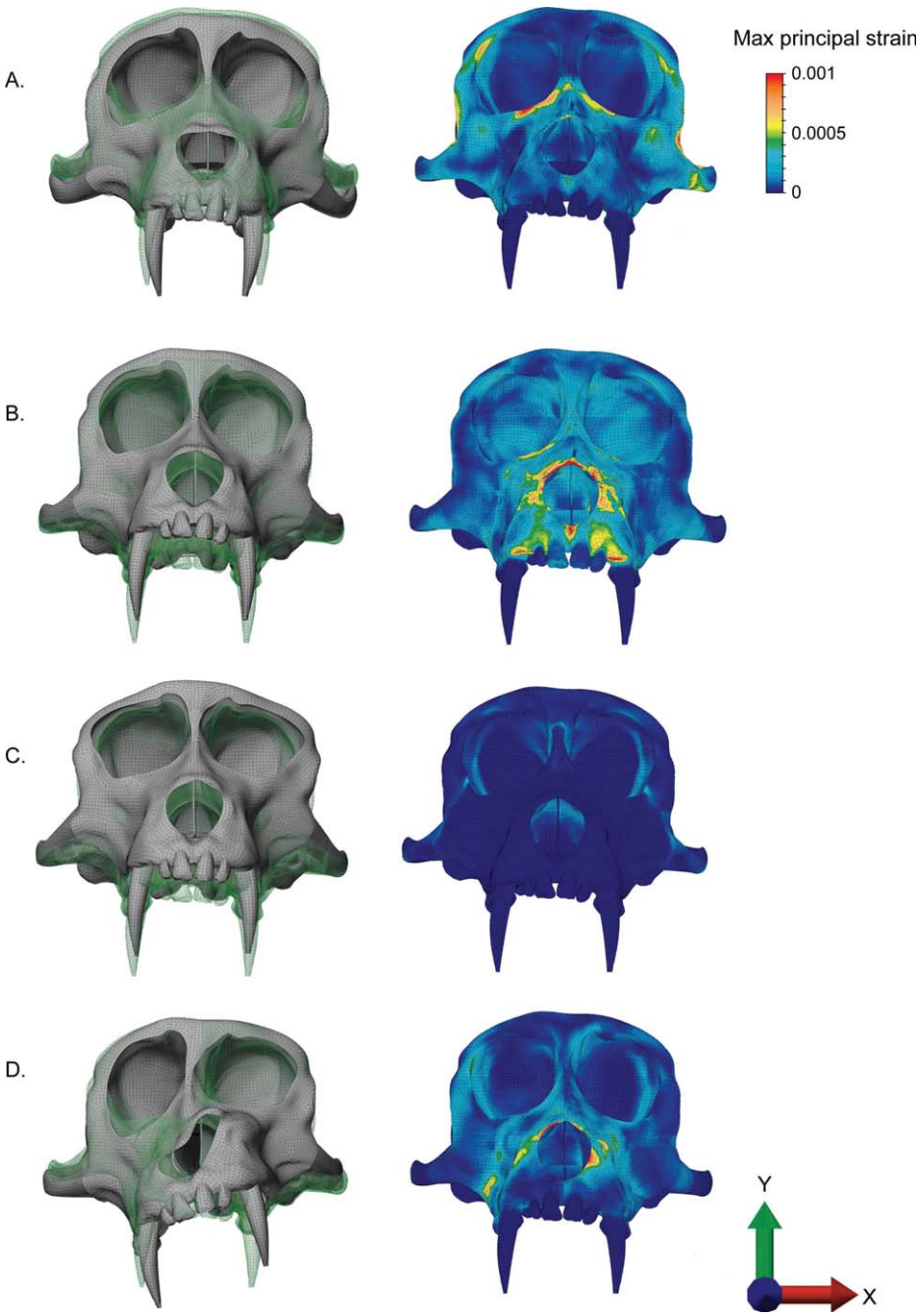


**Fig. 3.** Maximum principal strain results from the finite element analysis of each model. The deformation relative to the original model and strain map of the maximum principal strain magnitude on an undeformed model are shown. The deformed model is scaled to 5% of model size. (**A**) Frontal plane bending FEM; (**B**) Sagittal plane bending FEM; (**C**) Dorsoventral shear FEM; and (**D**) Torsion FEM.

bital (Node 2) regions. The frontal bending, sagittal bending, and validated FEMs fall within the variation from experimental data at the balancing side zygomatic arch (Node 7). The validated FEM and frontal bending models are within the experimental dispersion for three additional locations including the balancing side orbital, balancing side infraorbital, and working side zygomatic arch (Nodes 3, 5, and 6). Although the validated FEM and the frontal bending model exhibit similar $\varepsilon_1/|\varepsilon_2|$ ratios in the working side infraorbital (Node 4), both FEMs exceed the experimental range at this location.

Euclidean distances between the $\varepsilon_1$ orientations confirm that the strain pattern of the frontal bending model most closely matches the validated FEM for five of the eight nodes, whereas the torsion model deforms in a manner distinct from the validated FEM at seven of eight nodes (Table 2).

Overall strain orientations from the superior and lateral aspects of the face (Fig. 6A) and anteroposterior transects along the rostrum (Fig. 6B) from the frontal bending FEM best approximate those observed in the validated FEM. However, strain orientations from the

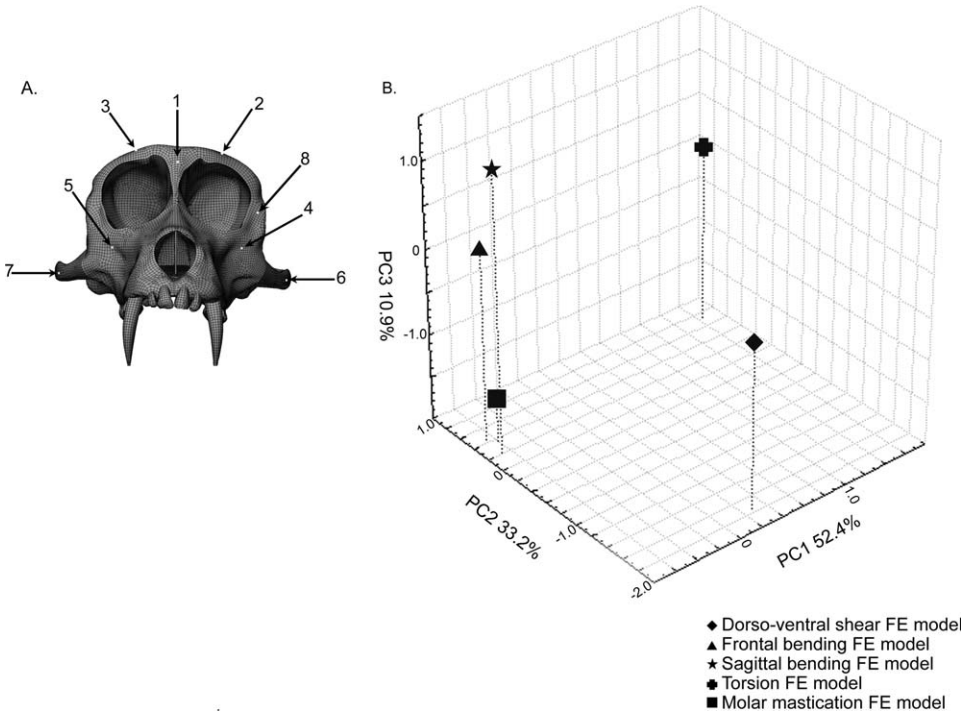


**Fig. 4.** (**A**) Macaque FEM illustrating the eight node locations for which experimental data were available. W = working side; B = balancing side; 1 = dorsal interorbital; 2 = W dorsal orbital; 3 = B dorsal orbital; 4 = W infraorbital; 5 = B infraorbital; 6 = W midzygomatic; 7 = B midzygomatic; 8 = W postorbital bar; (**B**) Principal components analysis of maximum principal strain orientation from the eight nodes corresponding to *in vivo* locations.

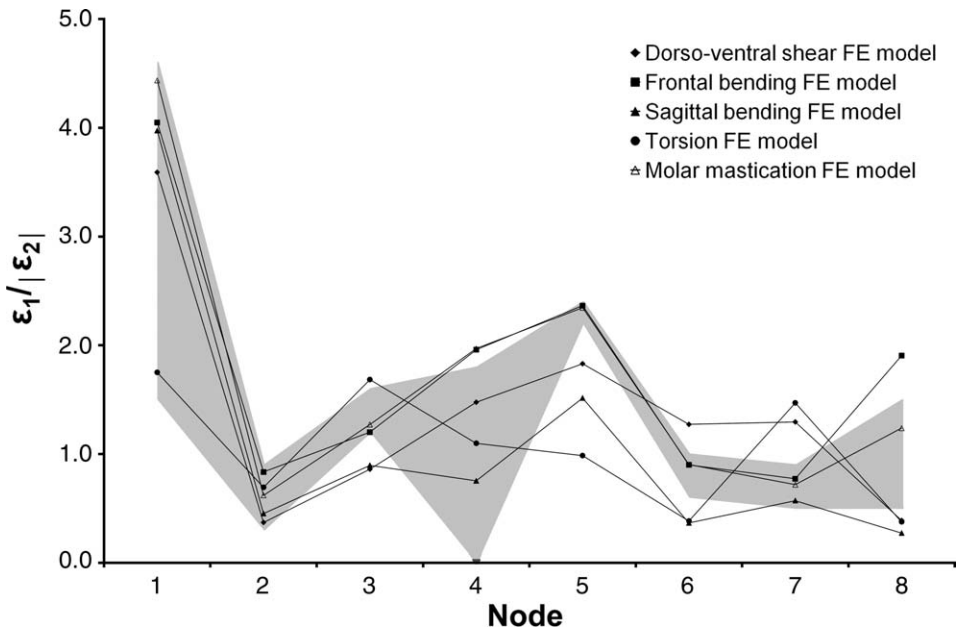


**Fig. 5.** Maximum to minimum principal strain ratio from the eight nodes corresponding to *in vivo* locations. The shaded area represents the dispersion of the experimental principal strain ratio data as reported by Strait et al. (2005).

area around the nasal aperture indicate none of the loading regime FEMs are comparable with the validated FEM (Fig. 6C). When maximum principal strain orientations from the working and balancing side nodes are considered separately, it seems that the working side (left side) deforms in a manner most similar to the torsion FEM, whereas the balancing side strain orientations exhibit a combination of torsion and sagittal bending.

## DISCUSSION

Our results do not support the first hypothesis, that simple geometric models provide accurate predictions of strain in the primate face. Comparisons of tensile strain predictions from simple geometric models (Fig. 1) with maximum principal strain magnitude in the FEMs (Figs. 3A-D) illustrate the inadequacy of these models to gener-

*TABLE 2. Summary of least-square distances of $\varepsilon_1$ orientation at each node corresponding to experimental gage locations*

| Node number | Region | Global loading regime FE model most similar to molar mastication FE model | Global loading regime FE model least similar to molar mastication FE model |
|---|---|---|---|
| 1 | Dorsal interorbital | Frontal bending | Torsion |
| 2 | W Dorsal orbital | Frontal bending | Torsion |
| 3 | B Dorsal orbital | Frontal bending | Torsion |
| 4 | W Infraorbital | Sagittal bending | Torsion |
| 5 | B Infraorbital | Frontal bending | Torsion |
| 6 | W Midzygomatic arch | Dorsoventral shear | Frontal bending |
| 7 | B Midzygomatic arch | Sagittal bending | Torsion |
| 8 | W Postorbital | Frontal bending | Torsion |

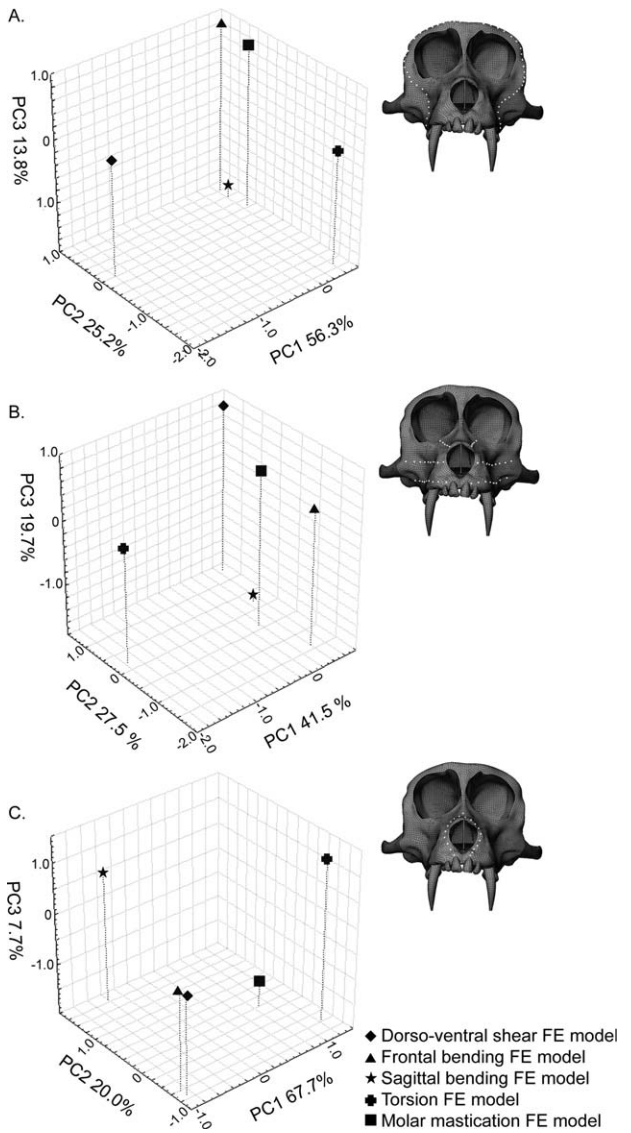


**Fig. 6.** Principal components analysis of maximum principal strain orientation from three additional nodal data sets. (**A**) A sample of nodes along the lateral and superior aspect of the face; (**B**) Three anteroposterior transects running along the working and balancing sides of the rostrum; (**C**) A sample running adjacent to nasal aperture.

ate strain predictions in the face—a conclusion also supported by previous cross sectional area, craniometric, and *in vivo* bone strain studies (Demes, 1982; Preuschoft et al., 1986; Ravosa, 1988; Hylander et al., 1991b; Ravosa, 1991; Hylander and Johnson, 1997; Ross, 2001). For instance, in the simple geometric model of sagittal bending, the skull is represented by a triangular-shaped beam. This model predicts a superiorly directed bite force and inferiorly directed muscle force will cause tensile strains along the palate, whereas compressive strains will be found along the dorsal aspect of the snout (Hylander et al., 1991b). The FEM of sagittal bending reveals a complex strain pattern not predicted by the simple geometric model. The FEM shows that concentrations of tension occur along portions of the maxilla superior to the nasal aperture during pure sagittal bending, but do not occur uniformly. Moreover, tensile strains also occur along the superior aspect of the nasal cavity, most likely due to folding of this curved sheet of maxillary bone surrounding the nasal aperture (Fig. 3B). Wang et al. (2010a) found that the presence of patent sutures serve to dampen strain in the surrounding cortical bone, whereas fused sutures and surrounding bone exhibit comparable strains. The long sutures in the snout may have patent sections which alter the strain patterns in this region during mastication. However, inconsistencies between the strain pattern observed in the sagittal bending FEM and the predictions of the simple geometric model are more likely the result of the geometric complexity of the sheets of bone comprising the snout.

The results presented here also do not support the hypothesis that a single global loading regime is primarily responsible for the pattern of craniofacial deformation in the macaque skull. Of the four regimes tested in this study, frontal bending yields $\varepsilon_1$ orientations and $\varepsilon_1/|\varepsilon_2|$ ratios that best approximate those experienced by the validated FEM. Frontal bending also most closely resembles the experimental bone strain data, falling within the dispersion of principal strain ratios collected from *in vivo* data. However, the loading regime showing the most similarity with the validated FEM and the experimental data varies with anatomical region. When strain orientations from the eight *in vivo* nodes were compared among the FEMs, no one global loading regime consistently matched the validated FEM. Likewise, strains produced during frontal plane bending match strains in the mastication model better in some anatomical regions (e.g., circumorbital region) than others (e.g., nasal margin). These results are consistent with the hypothesis that multiple regional loading regimes are present in the primate face during mastication (Hylander et al., 1991b; Ross and Hylander, 1996; Hylander and Johnson, 1997; Ross, 2001). Therefore, although the frontal bending model broadly predicts strains in the superior and lateral aspects of the face, it is apparent that none of the proposed global loading regimes alone sufficiently explains the strain pattern observed throughout the validated FEM.

In their study of the postorbital septum, Ross and Hylander (1996) noted that attempting to simplify complex facial loading patterns with simple global loading regimes is inaccurate, because local structures each experience unique combinations of loads and constraints. Before making assumptions about whether physiologic craniofacial strain patterns are best interpreted as the overall effects of simple global loading regimes, local geometry must be considered to elucidate local patterns of facial strain. Moreover, loading environments during orofacial function are usually asymmetric and vary within the same structure on working and balancing sides of the face. In the midzygomatic region, the working side midzygomatic arch experiences strain orientations that match the dorsoventral shear model, whereas the balancing side is most similar to the sagittal plane FEM. These observed differences in strain orientations between the working and balancing side zygomatics may be explained by differences in muscle activity between the deep and superficial parts of the masseter muscle (Hylander and Johnson, 1997). Strain orientation around the nasal aperture also varies from working to balancing side, with the balancing side deforming in a manner similar to predictions based on simple global loading regimes of both the torsion and sagittal bending models, compared with the working side which primarily resembles the torsion model. Generally, it seems that during mastication the superior and lateral face primarily resemble a simple bending model as a result of the influence of the masseter muscle, whereas more anterior regions of the face, such as the rostrum, are subject to complex combination of the bending and twisting models (Fig. 6). It is likely that for some discrete regions of the face, these global loading regimes are sufficient to describe strain patterns. However, understanding strain in FEMs of the entire facial skeleton requires more specific study of patterns of strain in smaller anatomical or functional regions so that multiple local complex skeletal geometries can be considered.

## CONCLUSION

Simple geometric models and terms describing simple deformation regimes of these models (e.g., bending in the frontal plane) while seemingly of heuristic value actually make imprecise and sometimes inaccurate predictions regarding strain distributions in the primate craniofacial skeleton. We propose that results from these oversimplified models be viewed with caution and be replaced when possible with FEMs, especially when used to interpret *in vivo* bone strain data. Finite element models more accurately capture complex craniofacial geometry and allow both regional and global comparisons within models. In the supplementary material, we provide maximum and minimum principal strain maps (Supplementary figs. 1, 2) and videos of the deformation (Supplementary figs. 3, 4) of our validated FE macaque model of molar mastication.

## ACKNOWLEDGMENTS

The authors thank Chris Ruff and the anonymous reviewers for their helpful comments on the manuscript.

## LITERATURE CITED

Antón SC. 1993. Internal masticatory muscle architecture in the Japanese macaque and its influence on bony morphology. Am J Phys Anthropol Suppl 16:50.

Antón SC. 1999. Macaque masseter muscle: internal architecture, fiber length and cross-sectional area. Int J Primatol 20:441–62.

Cartmill M. 1974. Daubentonia, Dactylopsila, woodpeckers, and klinorhychy. In: Martin R, Doyle G, Walker A, editors. Prosimian biology. London: Gerald Duckworth and Co. p 655–670.

Demes B. 1982. The resistance of primate skulls against mechanical stresses. J Hum Evol 11:687–691.

Dumont ER, Piccirillo J, Grosse IR. 2005. Finite-element analysis of biting behavior and bone stress in the facial skeletons of bats. Anat Rec Part A 283A:319–330.

Endo B. 1966. Experimental studies on the mechanical significance of the form of the human facial skeleton. J Fac Sci Tokyo Sect V 3:1–106.

Endo B. 1970. Analysis of stresses around the orbit due to masseter and temporalis muscle respectively. J Anthropol Soc Nippon 78:251–266.

Endo B. 1973. Stress analysis on the facial skeleton of Gorilla by means of the wire strain gage method. Primates 14:37–45.

Görke O. 1904. Beitrag zur funktionellen Gestaltung des Schädels bei den Anthropomorphen und Menchen durch Untersuchung mit Röntgenstrahlen. Arch Anthrop 1:91–108.

Greaves W. 1985. The mammalian postorbital bar as a torsion-resisting helical strut. J Zool 207:125–136.

Greaves W. 1995. Functional predictions from theoretical models of the skull and jaws in reptiles and mammals. Cambridge: Cambridge University Press.

Hylander W. 1977. The adaptive significance of Eskimo craniofacial morphology. In: Dahlberg A, Graber T, editors. Orofacial growth and development. The Hague: Mouton. p 129–69.

Hylander W, Johnson K. 1997. *In vivo* bone strain patterns in the zygomatic arch of macaques and the significance of these patterns for functional interpretations of craniofacial form. Am J Phys Anthropol 102:203–32.

Hylander WL, Picq PG, Johnson K. 1991a. Function of the supraorbital region of primates. Arch Oral Biol 36:273–281.

Hylander WL, Picq PG, Johnson K. 1991b. Masticatory-stress hypotheses and the supraorbital region of primates. Am J Phys Anthropol 86:1–36.

Kupczik K, Dobson CA, Crompton RH, Phillips R, Oxnard CE, Fagan MJ, O'Higgins P. 2009. Masticatory loading and bone adaptation in the supraorbital torus of developing macaques. Am J Phys Anthropol 139:193–203.

Kupczik K, Dobson CA, Fagan MJ, Crompton RH, Oxnard CE, O' Higgins P. 2007. Assessing mechanical function of the zygomatic region in macaques: validation and sensitivity testing of finite element models. J Anat 210:41–53.

Metzger KA, Daniel WJT, Ross CF. 2005. Comparison of beam theory and finite-element analysis with *in vivo* bone strain data from the alligator cranium. Anat Rec Part A 283A:331–348.

Picq PG, Hylander WL. 1989. Endo's stress analysis of the primate skull and the functional significance of the supraorbital region. Am J Phys Anthropol 79:393–398.

Preuschoft H, Demes B, Meyer M, Bar H. 1986. The biomechanical principles realized in the upper jaw of long-snouted primates. In: Else J, Lee P, editors. Primate evolution. Cambridge: Cambridge University. p 249–64.

Rangel R, Oyen O, Russell M. 1985. Changes in masticatory biomechanics and stress magnitude that affect growth and development of the facial skeleton. In: Dixon A, Sarnat B, editors. Normal and abnormal bone growth: basic and clinical research. New York: Alan R. Liss. p 281–293.

Ravosa M. 1988. Browridge development in *Cercopithecidae*: a test of two models. Am J Phys Anthropol 76:535–555.

Ravosa M. 1991. Interspecific perspective on mechanical and nonmechanical models of primate circumorbital morphology. Am J Phys Anthropol 86:369–396.

Rayfield EJ. 2007. Finite element analysis and understanding the biomechanics and evolution of living and fossil organisms. Ann Rev Earth Planet Sci 35:541–576.

Richmond BG, Wright BW, Grosse I, Dechow PC, Ross CF, Spencer MA, Strait DS. 2005. Finite element analysis in functional morphology. Anat Rec Part A 283A:259–274

Richter W. 1920. Monatssschr Der Obergesichtscädel des Menschen als Gebissturm, ein Statische Kunstwerk Dtsch Zahnheilkd 38:49–68.

Roberts D, Tattersall I. 1974. Skull form and the mechanics of mandibular elevation in mammals. Am Mus Novit 2536:1–9.

Ross CF. 2001. *In vivo* function of the craniofacial haft: the interorbital "pillar." Am J Phys Anthropol 116:108–139.

Ross CF. 2008. Does the primate face torque? In: Vinyard CJ, Ravosa M, Wall CE, editors. Primate craniofacial function and biology. New York: Springer. p 63–82.

Ross CF, Hylander W. 1996. *In vivo* and *in vitro* bone strain in the owl monkey circumorbital region and the function of the postorbital septum. Am J Phys Anthropol 101:183–215.

Ross CF, Patel BA, Slice DE, Strait DS, Dechow PC, Richmond BG, Spencer MA. 2005. Modeling masticatory muscle force in finite element analysis: sensitivity analysis using principal coordinates analysis. Anat Rec Part A 283A:288–299.

Ross CF, Strait D, Richmond B, and Spencer M. 2002. *In vivo* bone strain and finite-element modeling of the anterior root of the zygoma in Macaca. Am J Phys Anthropol Suppl 34: 133.

Ross CF, Strait DS, Dechow PC, Richmond BG, Spencer MS, Iriarte-Diaz J. (n.d.) *In vivo* bone strain and finite-element modeling of the craniofacial haft in catarrhine primates. J Anat, in press.

Russell M. 1985. The supraorbital torus: "A most remarkable peculiarity". Curr Anthropol 26:337–360.

StatSoft. 2006. STATISTICA, version 7.1, Tulsa, OK.

Strait DS, Grosse IR, Dechow PC, Smith AL, Wang Q, Weber GW, Neubauer S, Slice DE, Chalk J, Richmond BG, Lucas PW, Spencer MA, Schrein C, Wright BW, Byron C, Ross CF. 2010. The structural rigidity of the cranium of *Australopithecus africanus*: implications for diet, dietary adaptations, and the allometry of feeding biomechanics. Anat Rec 293:583–593.

Strait DS, Richmond BG, Spencer MA, Ross CF, Dechow PC, Wood BA. 2007. Masticatory biomechanics and its relevance to early hominid phylogeny: an examination of palatal thickness using finite-element analysis. J Hum Evol 52:585–599.

Strait DS, Wang Q, Dechow P, Ross C, Richmond B, Spencer M, Patel B. 2005. Modeling elastic properties in finite-element analysis: how much precision is needed to produce an accurate model? Anat Rec Part A 283A:275–287.

Strait DS, Weber GW, Neubauer S, Chalk J, Richmond BG, Lucas PW, Spencer MA, Schrein C, Dechow PC, Ross CF, Grosse IR, Wright BW, Constantino P, Wood BA, Lawn B, Hylander WL, Wang Q, Byron C, Slice DE, Smith AL. 2009. The feeding biomechanics and dietary ecology of *Australopithecus africanus*.. Proc Nat Acad Sci 106:2124–2129.

Wang Q, Dechow PC, Wright BW, Ross CF, Strait DS, Richmond BG, Spencer MA, Byron CD. 2008. Surface strain on bone and sutures in a monkey facial skeleton: an *in vitro* method and its relevance to finite element analysis. In: Vinyard CJ, Ravosa M, Wall CE, editors. Primate craniofacial function and biology. New York: Springer. p 149–172.

Wang Q, Smith AL, Strait DS, Wright BW, Richmond BG, Grosse IR, Byron CD, Zapata U. 2010a. The global impact of sutures assessed in a finite element model of a macaque cranium. Anat Rec 293:1477–1491.

Wang Q, Wright BW, Smith A, Chalk J, Byron CD. 2010b. Mechanical impact of incisor loading on the primate midfacial skeleton and its relevance to human evolution. Anat Rec 293:607–617.